

# Direct growth of aligned carbon nanotubes on bulk metals

S. TALAPATRA<sup>1,2\*</sup>, S. KAR<sup>1</sup>, S. K. PAL<sup>1</sup>, R. VAJTAI<sup>2</sup>, L. CI<sup>1</sup>, P. VICTOR<sup>1</sup>, M. M. SHAIJUMON<sup>1</sup>, S. KAUR<sup>1</sup>, O. NALAMASU<sup>1</sup> AND P. M. AJAYAN<sup>1,2</sup>

<sup>1</sup>Department of Materials Science & Engineering, Rensselaer Polytechnic Institute, 110 Eighth Street, Troy, New York 12180, USA

<sup>2</sup>Rensselaer Nanotechnology Center, Rensselaer Polytechnic Institute, 110 Eighth Street, Troy, New York 12180, USA

\*e-mail: talaps@rpi.edu

Published online: 22 October 2006; doi:10.1038/nnano.2006.56

There are several advantages of growing carbon nanotubes (CNTs) directly on bulk metals, for example in the formation of robust CNT–metal contacts during growth. Usually, aligned CNTs<sup>1–9</sup> are grown either by using thin catalyst layers predeposited on substrates<sup>1–7</sup> or through vapour-phase catalyst delivery<sup>7–9</sup>. The latter method, although flexible, is unsuitable for growing CNTs directly on metallic substrates. Here we report on the growth of aligned multiwalled CNTs on a metallic alloy, Inconel 600 (Inconel), using vapour-phase catalyst delivery. The CNTs are well anchored to the substrate and show excellent electrical contact with it. These CNT–metal structures were then used to fabricate double-layer capacitors and field-emitter devices, which demonstrated improved performance over previously designed CNT structures. Inconel coatings can also be used to grow CNTs on other metallic substrates. This finding overcomes the substrate limitation for nanotube growth which should assist the development of future CNT-related technologies.

Carbon nanotubes (CNTs) offer promising applications in fields ranging from electronics to biotechnology<sup>10–12</sup>. The development of techniques for controlled, aligned CNT growth on suitable substrates<sup>1–10,12,13</sup> has received special attention as well-defined CNT architectures are important for applications<sup>10,13–15</sup> such as displays, gigascale interconnects and micro/nanosensors. For most of these applications, appropriate structures with high-quality CNT–metal contacts are needed. The most obvious way to generate such structures would be to grow CNTs directly on bulk metals. However, CNTs are known to grow predominantly on nonconducting substrates, posing restrictions on applications where conductive substrates/contacts are required. This difficulty is only partially circumvented by using catalyst-printed metals<sup>5–7</sup>, through difficult multistage processes or post-growth metallization techniques, or other complex methods using voltage bias in methane inverse diffusion flames to grow CNTs on transition metal alloys<sup>16</sup>, or by high-temperature surface conditioning of steel to grow CNTs on them<sup>17</sup>. Vapour-phase catalyst delivery is an easier, scalable and versatile technique for obtaining well-organized, three-dimensional architectures of aligned CNTs, but it is selective only for non-conductive substrates<sup>8,9</sup>. Thus, it is important to either develop new processes for nanotube growth on metals or to identify suitable metals on which nanotubes can be grown easily with the available technologies. In this letter we present the direct growth of aligned nanotubes on Inconel by a vapour-phase catalyst delivery

chemical vapour deposition (CVD) method. Arrays of well-aligned multiwalled CNTs were grown on a variety of as-received Inconel substrates. The CNT–Inconel interface exhibits good electrical contact as well as strong mechanical adhesion and can be used directly as an electrode for supercapacitors and robust field emitters without any post-growth processing.

Figure 1 presents images of aligned multiwalled nanotubes (MWNT) grown on Inconel. Figure 1a is an optical image of the different substrates used for nanotube growth. A scanning electron microscope (SEM) image of CNTs grown on a mechanically deformed Inconel sheet is shown in Fig. 1b. Figure 1c, e shows corner and side views, respectively, of aligned nanotubes along an edge of an Inconel sheet, and Fig. 1d shows nanotubes grown on an Inconel wire. A high-resolution transmission electron microscopy (HRTEM) image of the nanotube is presented in Fig. 1f, showing the well-graphitized walls of the MWNTs. The high degree of crystallinity of a nanotube was also verified from Raman spectroscopy, which showed a strong G band at  $\sim 1,580 \text{ cm}^{-1}$  and a D band at  $\sim 1,349 \text{ cm}^{-1}$  (see Supplementary Information). The nanotube growth on Inconel provides at least two major advantages. First, the growth is not spatially restricted by the presence of a catalyst (as in the case of catalyst-deposited metal substrates), thus providing a way to fabricate three-dimensionally aligned nanotube arrays on metals in a single step. Second, the ability to grow nanotubes on any shape or size of substrate provides tremendous flexibility for developing applications where the morphology of the conductive substrates is critical.

For seamless integration into different technologies, the nanotube–substrate interface should be mechanically strong and electrically transparent. The shear adhesion strength determined for a nanotube–wire assembly (Fig. 2a) was found to be  $\sim 0.26 \text{ MPa}$ , which is similar to the adhesion strength of as-produced nanotubes on silicon carbide ( $\sim 0.27 \text{ MPa}$ ; ref. 13). The current–voltage ( $I$ – $V$ ) characteristics through the nanotube–Inconel interface are shown in Fig. 2b. Figure 2c shows the temperature dependence of the zero-bias conductance,  $G_0 = dI/dV|_{V=0}$ , below 100 K.  $G_0$  is found to vary linearly with  $T^{1/2}$  down to  $T = 40 \text{ K}$ , below which it has a slower  $T$ -dependence. These observations are similar to those for single<sup>18</sup> and isolated aligned arrays of MWNTs<sup>19</sup>, possibly because individual nanotubes in the mat conduct independently, without any significant lateral transport. In such an array of resistors, the

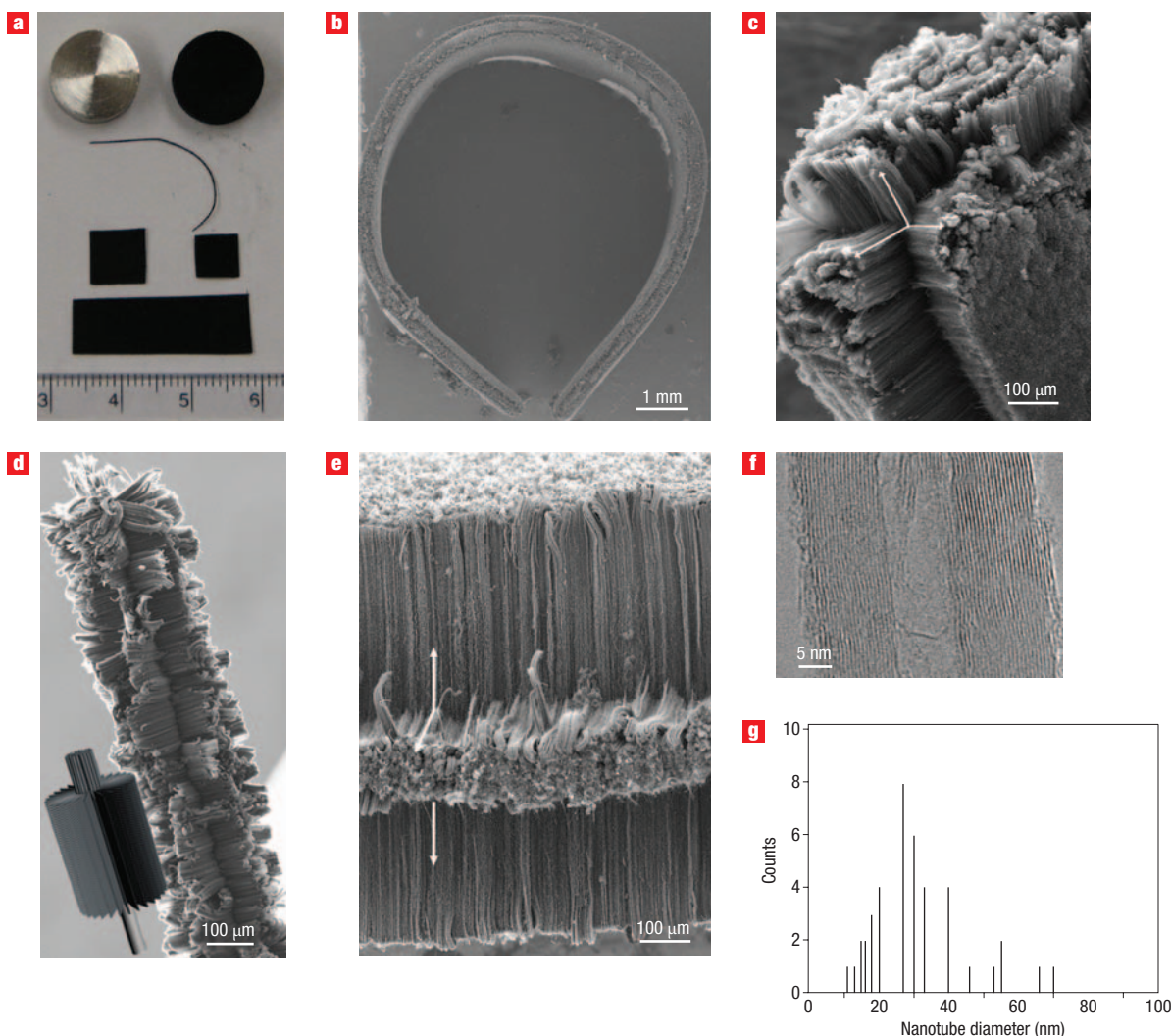


**Figure 1** Aligned MWNTs grown on different geometries of Inconel substrates. **a**, Optical image of differently shaped and sized Inconel substrates used for CNT growth. The top-left and top-right examples are the as-received Inconel rod and a similar substrate with uniform CNTs grown on it. An Inconel wire and sheets are also shown. The scale along the bottom is in cm. **b**, SEM image of CNTs grown on a mechanically deformed Inconel sheet (0.2 mm thick), showing that the substrate can be given any shape and be used for CNT growth. **c**, SEM image showing the corner of a CNT-grown Inconel sheet. Note the highly directional nature of the CNT growth, with the orientation of the nanotubes being perpendicular to the substrate surface. The arrows indicate the direction of CNT growth. **d**, SEM image of nanotubes grown on an Inconel wire of diameter 50  $\mu\text{m}$ . A schematic showing the brush structure on the wire is shown in the inset. **e**, SEM image of one side of an Inconel sheet (0.075 mm thick) showing well-aligned CNTs on the top, side and bottom of the substrate. The arrows indicate the direction of CNT growth. **f**, HRTEM image of a typical grown nanotube, showing the well-graphitized walls of the MWNT. **g**, Typical diameter distribution of nanotubes, determined from TEM.

total resistance is smaller than that of the smallest individual resistor (comprising a tube and its interface resistance), which is probably the nanotube with the most dominant metallic MWNT–interface. The linearity of the  $I$ – $V$  curves down to 20 K suggests the formation of ohmic junctions at the growth interface of at least the most metallic nanotubes in the forest.

Metal–nanotube interfaces are known to have large contact resistances. From a technological perspective, the total resistance of a via/interconnect structure dominates important performance parameters such as delay and power dissipation in large-scale integration. With this in mind, the resistance of nanotube pillars grown directly on Inconel was measured using a micromanipulator probe top contact (tip size  $\sim 10 \mu\text{m}$ ). The average total resistance (including the contact resistance) measured over many such pillars was found to be  $\sim 500 \Omega$  (see Supplementary Information),

suggesting good electrical contact between the nanotubes and the metal substrate.

To demonstrate the impact of good electrical contact between CNT and metal on device performance, we have measured the capacitive behaviour (Fig. 3) of a double-layer capacitor (DLC) fabricated using the Inconel substrate with aligned nanotubes as electrodes. Figure 3b shows the cyclic voltammograms (CVs) of the DLC at various scan rates. An impressive device property is readily realized from these measurements. The rectangular and symmetric shape of the CVs performed at high scan rates of  $1,000 \text{ mV s}^{-1}$  (a typical ideal capacitive behaviour<sup>20,21</sup>) suggests low contact resistance between the CNTs and Inconel. Lowering the contact resistance between the nanotubes and collector electrodes in DLCs has been a major issue in developing CNT-based supercapacitors, and is typically achieved by mixing nanotubes

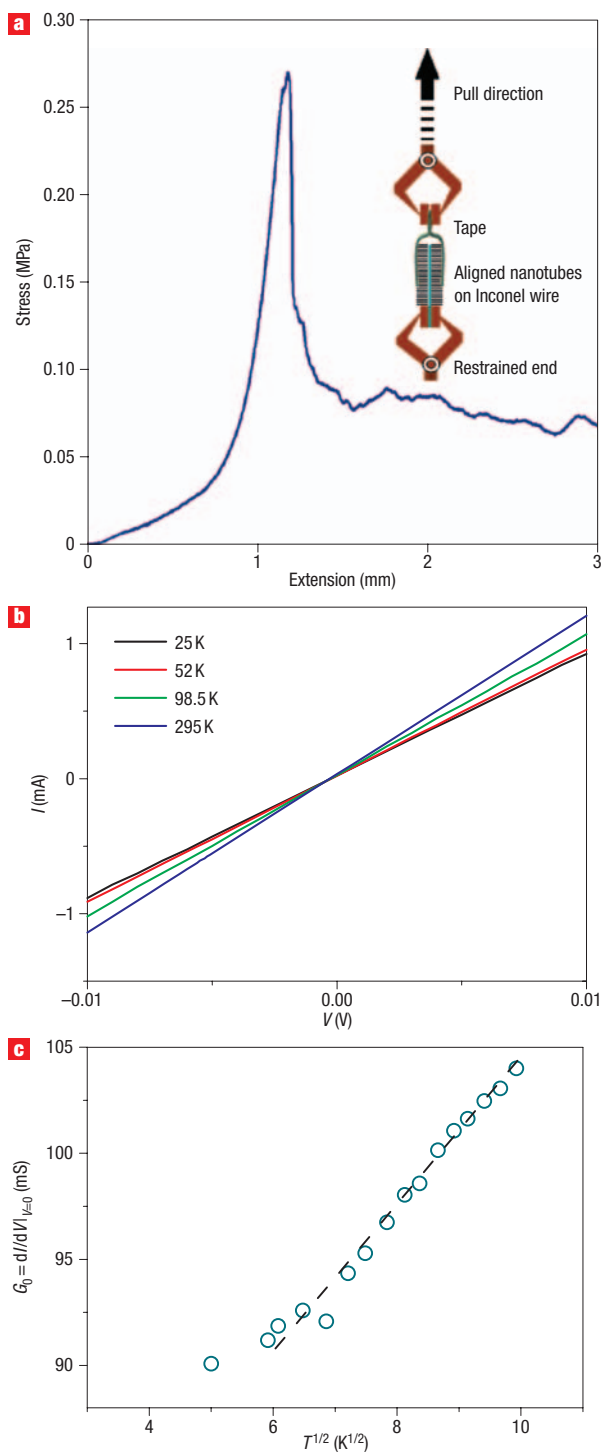


**Figure 2** Mechanical and electrical characterization of the CNT–Inconel interface. **a**, Shear stress as a function of displacement, used to determine the adhesion strength of the nanotubes grown on the Inconel wire. The inset shows a schematic of the setup used for performing the measurement. **b**,  $I$ – $V$  measurements performed on the CNT–Inconel structure at various temperatures. The data show that the resistance of this structure increases monotonically with a decrease in temperature from  $\sim 300$  K to  $\sim 20$  K. The  $I$ – $V$  characteristics remain nearly linear at all temperatures, with a slight increase in nonlinearity at the lowest temperatures. Below  $T = 30$  K, the dynamic conductance  $G = dI/dV$  begins to show a very small dip (not shown) at zero bias. **c**, Temperature dependence of the zero-bias conductance  $G_0$  below 100 K.

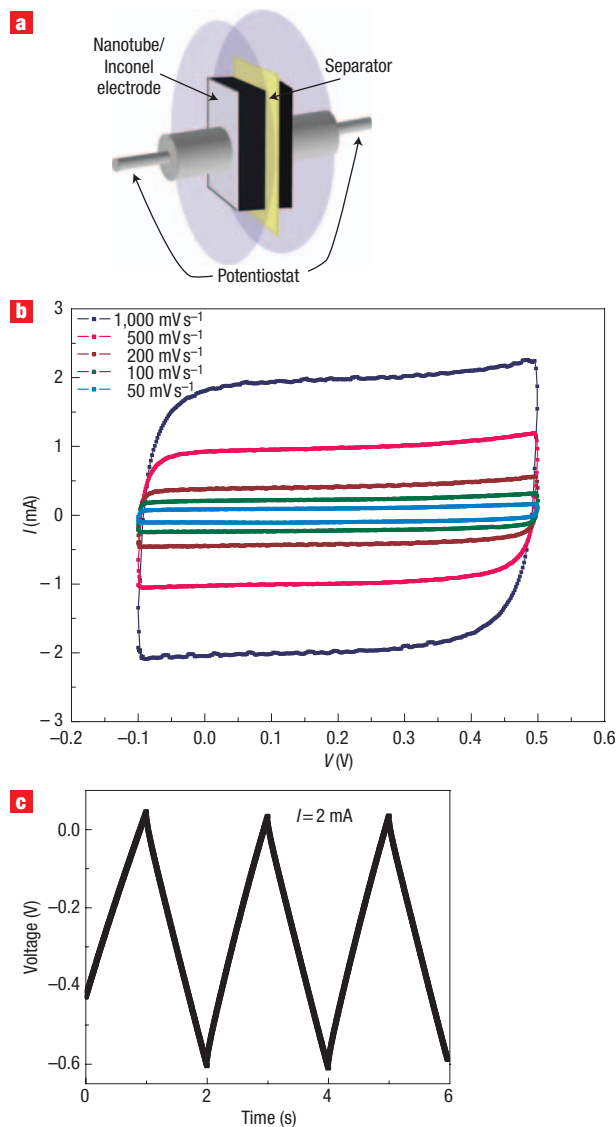


**Figure 3** Double-layer capacitor measurements of CNT–Inconel sheets. **a**, The experimental arrangement used to fabricate and measure the DLC properties of the CNT–Inconel electrodes. **b**, Cyclic voltammograms measured for a particular DLC device at scan rates ranging from  $50 \text{ mV s}^{-1}$  to  $1,000 \text{ mV s}^{-1}$ . The rectangular shape of the CVs are maintained, even at very high scan rates. The CV data obtained at  $1,000 \text{ mV s}^{-1}$  were used for calculating the specific power density of the device (reported in the main text). **c**, Charge–discharge cycles taken at a constant current of 2 mA. The discharge slope was used to calculate the specific capacitance of the device.

with conductive binders and coating collector electrodes with this composite. This process drastically modifies nanotube electrode properties<sup>20</sup>, leading to adverse effects on the performance of the DLC. In our capacitors, because the nanotubes are directly grown on the electrodes, this problem does not arise. The specific capacitance value for the DLCs, calculated from the discharge slope measured at 2 mA (Fig. 3c), was found to be  $18 \text{ F g}^{-1}$  (comparable to the values obtained for DLCs fabricated using CVD-grown MWNT<sup>21</sup>), with a power density of  $\sim 7 \text{ kW kg}^{-1}$  at  $1,000 \text{ mV s}^{-1}$  scan rate. The high value of the power density is well suited for surge-power delivery applications<sup>20,21</sup>.

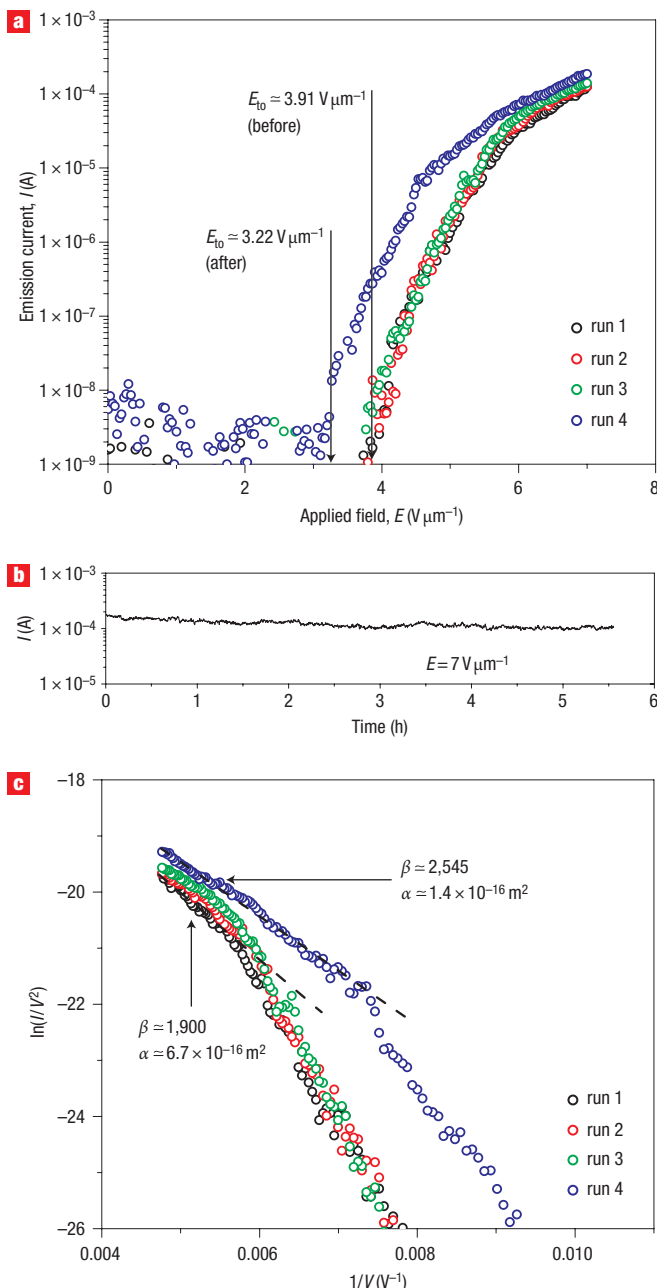


**Figure 4** Field-emission characteristics of the CNT–Inconel electrodes.

**a**, Variation of the emission current as a function of the applied field for several runs obtained for a particular device. One measurement (run 4) performed after the reliability test (**b**) is also included in the figure. The emission current was found to improve marginally with each cycle (see runs 1–3), due to the removal of adsorbed species and/or realignment of the tubes under the high temperature and electrostatic forces. **b**, On-state operation of a particular device (at a fixed field of  $E = 7 \text{ V } \mu\text{m}^{-1}$ ). The stability of the emission current at the highest applied field over long hours of operation is shown. **c**, Fowler–Nordheim plots obtained for each run. The curves show at least two distinct slopes, attributed to a non-metal-like emission process from discrete energy states, often seen in nanotubes. This is usually associated with the release of photons with a blackbody spectrum. The field-enhancement factors ( $\beta$ -values) were estimated for high field operation conditions from the Fowler–Nordheim plot. The effective area of emission,  $\alpha$ , decreases from  $\sim 6.7 \times 10^{-16} \text{ m}^2$  to  $1.4 \times 10^{-16} \text{ m}^2$  after the reliability test, indicating that the emission is occurring from a single nanotube whose tip becomes sharper during the few hours of emission.

CNTs are known for their field-emission properties<sup>12,22,23</sup>. MWNTs grown directly on Inconel form a single-step composite cathode for field emission. Figure 4a presents the emission current as a function of applied voltage in a typical device, measured over successive cycles. These devices were extremely reliable over several hours (Fig. 4b). Field emission measured after this reliability test showed a lowering of the turn-on field  $E_{\text{to}}$  (where current exceeded 10 nA) from  $3.91 \text{ V } \mu\text{m}^{-1}$  to  $3.22 \text{ V } \mu\text{m}^{-1}$  for the device under consideration. The corresponding field-enhancement factors  $\beta$  (determined from a Fowler–Nordheim plot, Fig. 4c) increased from  $\beta \approx 1,900$  before the reliability test to  $\beta \approx 2,500$  afterwards. With time, the emission parameters modify, as seen in earlier work<sup>24</sup>, but the electrical contact between the nanotubes and Inconel remains stable. The field enhancement and turn-on field can be significantly improved by isolating the emitting tips (and hence decreasing the mutual screening<sup>22</sup>) from the bulk of the nanotube forest by infiltration of an insulating matrix<sup>22</sup>.

We have further tested the suitability of thin layers (several hundreds of nanometres thick) of Inconel deposited on other metallic substrates for nanotube growth. Aligned growth of nanotubes was obtained on patterns of Inconel deposited on Au as well as Inconel-coated Be–Cu alloy wires (see Supplementary Information). This outcome certainly removes substrate limitation for nanotube growth and opens up the possibility for aligned nanotube growth on a large spectrum of conductive substrates.

Previous studies have shown that the catalyst–substrate interaction plays a crucial role in CNT growth<sup>25</sup>. For example, growth occurs on  $\text{SiO}_2$  and not on Si, because of a strong interaction of the catalyst with Si. In general, a strong substrate–catalyst interaction inhibits CNT growth. Minimal surface diffusion and formation of high-density catalyst nanoparticles<sup>26</sup> (but not a continuous film) on the substrate is another important criterion for providing nucleation sites for CNT growth. We believe that these factors balance out optimally in Inconel to facilitate formation of stable catalyst particles, resulting in CNT growth, as opposed to other substrates such as Si, Au or Cu. As a general strategy, alloys comprising more than one metal (such as Al, Cu, Co, Cr, Fe, Ni, Pt, Ta, Ti, Zn) could also support CNT growth.

In conclusion, we have shown that aligned nanotube arrays with strong mechanical adhesion and low contact resistance can be grown directly on Inconel substrates using the floating-catalyst CVD method. The oxidation resistance of Inconel is advantageous both for growth and for high-temperature applications. Realistic devices were fabricated using these substrates. Electrically end-contacted<sup>27,28</sup> dense bundles of aligned CNTs are promising candidates for interconnects and via structures at the sub-50-nm technology node<sup>29</sup>. For optimal performance in these architectures, any metallization of individual tubes has to be on their ends, such that individual shells can be accessed by each electrode, and each nanotube in the bundle has to be individually metallized in this way. Post-growth metallization techniques are yet to reliably meet these criteria on a large scale. The unique advantage of the direct growth of nanotubes on metallic substrates is that, within the array, every individual nanotube is electrically end-connected *in situ*, overcoming several obstacles to applications in interconnect and contact technologies, field emitters and supercapacitors.

## METHODS

### NANOTUBE GROWTH

We used a ferrocene–xylene CVD system for the growth of vertically aligned CNTs directly onto an Inconel 600 substrate. A solution made by dissolving 1 g of ferrocene in 100 ml of xylene was injected into a preheated steel bottle

(210 °C) with a syringe pump. A constant pumping speed of 0.11 ml min<sup>-1</sup> was maintained while injecting this solution into the bottle. An Ar/H<sub>2</sub> mixture (85% Ar) carried the xylene vapour containing the catalyst at 100 s.c.c.m. before entering the furnace. The furnace containing the Inconel substrates was maintained at 770 °C. The major reported constituents of the substrates were 72% Ni, 16% Cr and 8% Fe.

#### ELECTRICAL TRANSPORT

Two-probe *I*–*V* characteristics were obtained for the CNT–Inconel electrodes at different representative temperatures under vacuum ( $\sim 5 \times 10^{-6}$  torr), in large area patterns ( $\sim 3$  mm) made by coating Ti/Cu electrodes on the top surface of the nanotube array. A wire was soldered directly onto the Inconel. The top of the nanotube array was electrically contacted by placing a thin Cu sheet (mounted on the ends of a spring-loaded probe) over the metal spot. The sample was then placed on a temperature-controlled cold stage for measurement of the *I*–*V* characteristics (for 20 K < *T* < 300 K). Repeated cycles of measurements were performed to check the consistency of the data.

#### ADHESION STRENGTH

The adhesion test between the aligned nanotube forest and the Inconel wire was carried out in an Instron 5803 electromechanical tester. One end of the wire containing the nanotubes was wrapped with adhesive tape. During the testing, the tape grabbed the nanotubes and was moved away at a constant speed of 1 mm min<sup>-1</sup> until the CNTs detached from the wire. The contact area used for determining the stress was the geometrical area of the cylindrical surface of the Inconel wire covered with the tape.

#### CAPACITANCE

The electrochemical properties and capacitance measurements of the electrodes were studied in a two-electrode system using 6 M KOH solution as the electrolyte. The electrodes were sandwiched in a Swagelok-type stainless-steel test cell with a Whatman filter paper immersed in the electrolyte as the separator. Cyclic voltammetry and galvanostatic charge–discharge measurements were carried out using a Potentiostat/Galvanostat (EG&G Princeton Applied Research, Model 273A). Voltammetry testing was carried out at potentials between –0.1 V and 0.5 V. For calculating the specific capacitance, the galvanostatic charge–discharge behaviour of the MWNTs was measured with an applied constant current of 2 mA over a time interval of 1 s. The specific capacitance was evaluated from the slope of the charge–discharge curves, according to

$$C_{\text{sp}} = \frac{I}{m(dV/dt)},$$

where *I* is the applied current and *m* is the mass of each electrode.

#### FIELD EMISSION

For the field-emission measurements, a metal anode with an adjustable separation distance was positioned parallel to the top surface of the aligned nanotubes. The spacing between the metal anode and the nanotube mat was set to  $\sim 30$  μm. The field-emission measurements were performed under a vacuum of  $\sim 2.2 \times 10^{-6}$  torr by applying a voltage from 0 V to 210 V between the two electrodes and measuring the current.

Received 1 June 2006; accepted 29 August 2006; Published 22 October 2006.

#### References

- Li, W. Z. *et al.* Large scale synthesis of aligned carbon nanotubes. *Science* **274**, 1701–1703 (1996).
- Ren, Z. F. *et al.* Synthesis of large arrays of well-aligned carbon nanotubes on glass. *Science* **282**, 1105–1107 (1998).
- Andrews, R. *et al.* Continuous production of aligned carbon nanotubes: a step closer to commercial realization. *Chem. Phys. Lett.* **303**, 467–474 (1999).
- Huczko, A. Synthesis of aligned carbon nanotubes. *Appl. Phys. A* **74**, 617–638 (2002).
- Wang, B. *et al.* Controllable preparation of patterns of aligned carbon nanotubes on metals and metal-coated silicon substrates. *J. Mater. Chem.* **13**, 1124–1126 (2003).
- Kind, H. *et al.* Patterned films of nanotubes using microcontact printing of catalysts. *Adv. Mater.* **11**, 1285–1289 (1999).
- Ng, T. H. *et al.* Growth of carbon nanotubes: a combinatorial method to study the effects of catalysts and underlayers. *J. Phys. Chem. B* **107**, 8484–8489 (2003).
- Terrones, M. *et al.* Controlled production of aligned-nanotube bundles. *Nature* **388**, 52–55 (1997).
- Wei, B. Q. *et al.* Organized assembly of carbon nanotubes. *Nature* **416**, 495–496 (2002).
- Dresselhaus, M. S., Dresselhaus G. & Avouris, P. (eds). *Carbon Nanotubes: Synthesis, Structure, Properties and Applications* (Springer, Heidelberg, 2001).
- Jarillo-Herrero, P., van Dam, J. A. & Kouwenhoven, L. P. Quantum supercurrent transistors in carbon nanotubes. *Nature* **439**, 953–956 (2006).
- Fan, S. *et al.* Self-oriented regular arrays of carbon nanotubes and their field emission properties. *Science* **283**, 512–514 (1999).
- Cao, A., Vinod, V., Li, X., Yao, Z., Ghasemi-Nejhad, M. & Ajayan, P. M. Multifunctional brushes made from carbon nanotubes. *Nature Mater.* **4**, 540–545 (2005).
- Teo, K. B. K. *et al.* Carbon nanotubes as cold cathodes. *Nature* **437**, 968 (2005).
- Bandaru, P. R., Daraio, C., Jin, S. & Rao, A. M. Novel electrical switching behaviour and logic in carbon nanotube Y-junctions. *Nature Mater.* **4**, 663–666 (2005).
- Xu, F., Liu, X. & Tse, S. Synthesis of carbon nanotubes on metal alloy substrates with voltage bias in methane inverse diffusion flames. *Carbon* **44**, 570–577 (2006).
- Karwa, M., Iqbal, Z. & Mitra, S. Scaled-up self assembly of carbon nanotubes inside long stainless steel tubing. *Carbon* **44**, 1235–1242 (2006).
- Graugnard, E., de Pablo, P. J., Walsh, B. A., Ghosh, W., Datta, S. & Reifengerger, R. Temperature dependence of the conductance of multiwalled carbon nanotubes. *Phys. Rev. B* **64**, 125407 (2001).
- Davydov, D. N., Li, J., Shelimov, K. B., Haslett, T. L., Moskovits, M. & Statt, B. W. Resistance and tunneling spectra of aligned multiwalled carbon nanotube arrays. *J. Appl. Phys.* **88**, 7205–7208 (2000).
- Burke, A. Ultracapacitors: why, how, and where is the technology. *J. Power Sources* **91**, 37–50 (2000).
- Du, C., Yeh, J. & Pan N. High power density supercapacitors using locally aligned carbon nanotube electrodes. *Nanotechnology* **16**, 350–353 (2005).
- Jung, Y. *et al.* Aligned carbon nanotube polymer hybrid architectures for diverse flexible electronic application. *Nano Lett.* **6**, 413–418 (2006).
- Sveningsson, M., Jönsson, M., Nerushev, O. A., Rohmund, F. & Campbell, E. E. B. Blackbody radiation from resistively heated multiwalled carbon nanotubes during field emission. *Appl. Phys. Lett.* **81**, 1095–1097 (2002).
- Sveningsson, M. *et al.* Raman spectroscopy and field-emission properties of CVD-grown carbon-nanotube films. *Appl. Phys. A* **73**, 409–418 (2001).
- Jung, Y. J., Wei, B. Q., Vajtai, R., Ajayan, P. M., Homma, Y., Prabhakaran, K. & Ogino, T. Mechanism of selective growth of carbon nanotubes on SiO<sub>2</sub>/Si patterns. *Nano Lett.* **3**, 561–564 (2003).
- Liu, C., Cheng, A., Clark, M. & Tzeng, Y. Effects of interfacial layers on thermal chemical vapour deposition of carbon nanotubes using iron catalyst. *Diam. Relat. Mater.* **14**, 835–840 (2005).
- Nihei, M., Horibe, M., Kawabata, A. & Awano, Y. Simultaneous formation of multiwall carbon nanotubes and their end-bonded ohmic contacts to Ti electrodes for future ULSI interconnects. *Jap. J. Appl. Phys.* **43**, 1856–1859 (2004).
- Kreupl, F., Graham, A. P., Liebau, M., Duesberg, G. S., Seidel, R. & Unger, E. Carbon nanotubes for interconnect applications. <http://arxiv.org/ftp/cond-mat/papers/0412/0412537.pdf>
- Naeemi, A., Sarvari, R. & Meindl, J. D. Performance comparison between carbon nanotube and copper interconnects for gigascale integration (GSI). *IEEE Electron. Device Lett.* **26**, 84–86 (2005).

#### Acknowledgements

We acknowledge funding support received from the RPI Nanoscale Science and Engineering Initiative of the National Science Foundation under NSF Grant No. DMR-0117792 and the Interconnect Focus Center New York at RPI. S.T. thanks X. Li for helpful discussions.

Correspondence and requests for materials should be addressed to S.T.

Supplementary information accompanies this paper on [www.nature.com/naturenanotechnology](http://www.nature.com/naturenanotechnology).

#### Competing financial interests

The authors declare that they have no competing financial interests.

Reprints and permission information is available online at <http://npg.nature.com/reprintsandpermissions/>